UNSTEADY LOW ASPECT RATIO CAVITY CONVECTION DRIVEN BY DIFFERENTIAL FLUXES ON THE HORIZONTAL BOUNDARIES *

Jeffrey J. Sturman
Department of Environmental Engineering and Centre for Water Research
University of Western Australia
Nedlands, Western Australia
Australia

Gregory N. Ivey
Department of Environmental Engineering and Centre for Water Research
University of Western Australia
Nedlands, Western Australia
Australia

ABSTRACT

The geophysically important horizontal exchange flows which are caused by spatial variation in heat fluxes acting on the surface of lakes and oceans, for example, are modelled by laboratory experiments in a low aspect ratio tank. The filling time is an important timescale in these flows, as in the field, heat fluxes often change at this or lesser timescales. The tank enables this important feature to be simulated by switching the signs of the buoyancy fluxes induced at the tank ends from producing destabilising convection to producing stabilising convection. Both experiments and scaling arguments show that the destabilising case gives overwhelmingly greater volume fluxes and hence transport of heat and passive tracers.

1. INTRODUCTION

Convection driven by spatially variable heat transfer across the water surface is an important forcing mechanism in driving horizontal exchange flows in geophysical applications such as lakes and reservoirs (Monismith, Imberger & Morison 1990), the polar oceans (Noh, Fernando & Ching, 1992) and sea breeze flows (Linden & Simpson 1986) to name a few. Although the causes of the differential turbulent heat fluxes vary in these situations, the consequences are the same: the creation of horizontal temperature and hence density gradients in the near surface regions which, in turn, drive horizontal flows. Such flows transport not only heat but also passive tracers such as chemical and biological species, and parameterizing these horizontal transports is essential to modelling exchange and flushing processes. While important, field observations of these flows are both difficult and costly to make.

Accordingly, we conducted an initial series of laboratory experiments to study these flows at steady state in a small pilot experiment covering a limited range of the effective Rayleigh number, Ra^*, (Sturman, Ivey & Taylor 1992), later extended by Sturman, Ivey & Taylor (1995), both studies with unstable configurations for the forcing. We describe here results from a much larger scale facility where we investigate previously unexplored parameter ranges of Ra^*, aspect ratio $A=H/L$ and the ratio of the the tank height to the effective length of the heated (or cooled) region $C = H/l$, the governing dimensionless parameters. In addition, this study will focus on unsteady flow regimes induced by gross perturbations to the buoyancy flux due to sudden switching of the sign of the buoyancy forcing in the end regions. This yields results which are more applicable to quantifying horizontal exchange flows in the various field situations indicated above, where the unsteady nature of the forcing is an important characteristic of the flow.

2. EXPERIMENTAL APPARATUS AND METHODS

The shallow rectangular tank has an aspect ratio of 0.05 based on depth to length; see Fig. 1 for a schematic diagram. Heat fluxes are applied by circulating water through jackets behind the horizontal copper plates 250mm long located at the top of one end of the tank and at the bottom of the other end. Switching the sign of the buoyancy flux at the plates is possible by using two connected four-way valves which enable heated and chilled water to be switched from one water jacket to the other. The tank was constructed of 19 mm perspex sheet and insulated with 50mm of polystyrene foam. Temperatures within the tank were measured by rapid response thermistor traverses, of one second duration, from tank top to bottom, taking 50 samples per traverse. Velocities were measured by a PIV method with further details available in Stevens and Coates (1994).

---

* Centre for Water Research reference ED-1008-JJS.

3. SCALING

3.1 Reversing Buoyancy, Steady State

From Sturman *et al* (1995) the horizontal outflow velocity from the plates with destabilising buoyancy flux ($B\_$) is

$$u \sim (B\_l)^{1/3} \quad (1)$$

and the thickness of the outflow is

$$\delta \sim h \ . \quad (2)$$

The volume discharge with destabilising buoyancy flux, $Q\_ = u\delta$, can be expressed as

$$Q\_ = (\nu\kappa)^{1/2} Ra^{1/3} \quad (3)$$

where

$$Ra = B\_l^4 / (\nu\kappa)^{3/2} \quad (4)$$

is based upon the horizontal plate length, the extent of the forcing region.

When the buoyancy flux is stabilising (B_+), there is a laminar conduction of heat diffusing into the fluid until horizontal advection balances vertical diffusion in the heat equation. Similarly there is a viscous buoyancy balance in the momentum equation, which, together with $g' \sim B_+^{2/3} / \delta^{1/3}$, leads to the boundary layer thickness

$$\delta \sim \left(\nu^3 \kappa^3 l^6 / B_+^2 \right)^{1/14} \quad (5)$$

and

$$u \sim \left(\kappa^4 B_+^2 l / \nu^3 \right)^{1/7} \quad (6)$$

and hence the volume discharge with stabilising buoyancy flux is given by

$$Q_+ \sim \kappa Ra^{1/7} \quad (7)$$

The condition for $Q\_ > Q_+$ is that

$$Ra > 1/Pr^{21/8} \quad (8)$$

which is always satisfied for water. This implies that in the sidearm of a reservoir, for example, almost all volume exchange is done in the destabilising situation, and this is confirmed by the comparison of the maximum velocity in the unstable case above, ~10mms^{-1} with a cubic profile, while for the stable situation the maximum was about 0.7mms^{-1}, confined in two jets each occupying about 20% of the tank height.

4. DESCRIPTION OF THE FLOW

The flow in the tank is initiated with a destabilising buoyancy flux at the plates, ie, heating the bottom plate and cooling the top plate. This is maintained for approximately 6 filling times, then the buoyancy fluxes are reversed to the stabilising configuration and this is maintained for approximately 4 further filling times, after which the buoyancy fluxes are returned again to the unstable state. The filling time is the time taken for the fluid in the tank to pass once through the boundary layers on the end plates and is given by $t_f = u\delta / HL$, (Sturman *et al* 1995 and §3). Typical filling times using appropriate scales for the sidearm of a reservoir for example range over O(10^4) to O(10^5) s.

4.1 Destabilising Forcing

The velocity field in the end region is shown in Figs 2a to 2c. Fig 2a shows that unstable plumes from the cold plate (left end Fig. 1) have descended to the tank bottom at $t/t_f \approx 0.13$, compared with the plume penetrative timescale (t_d) scaled by the filling time $t_d / t_f \sim h/(B\_h)^{1/3} / t_f = 0.04$ (see §4). Significant local recirculations are visible at each end. In Fig 2b recirculating flow has penetrated about 2/3rds of the way along the cold plate at $t/t_f \approx 0.3$. By steady state ($t/t_f \approx 6$) Fig 2c shows recirculating flow has penetrated over whole plate. Note the flattened separation feature on the lower wall.

Note that Phillips (1966) similarity solution predicts $u \sim x^{1/3}$ (x measured from plate leading edge in this instance). This is not confirmed in the current experiment with data derived from Fig 2c, where $u \sim const.$ over most of the plate, rolling off quickly near the end wall. The reason for this is due to two factors: our tank is stratified at steady state, and the finite depth of our tank complicates the application of Phillip's similarity solutions. Globally, however, we find that this scaling still gives a correct discharge velocity scale from the plate end (see §3 above).

In the interior, the form of the velocity field is similar to that observed by Sturman *et al* (1995), ie a cubic profile, consistent with $B\_ > \nu^3 / (A^3 l^4)$, the condition for no quiescence at the centre as predicted by Sturman *et al* (1995). The maxima of the velocity profile is about 10mms^{-1} compared with the scaling prediction (see (1) above) of 8mms^{-1}.

The temperature field at $x/L = 0.5$ in the interior is shown in Fig 3. The passage of the intrusion gives a rough estimate of t_f, about 800s compared with the scaling estimate of 400s. Note that the maxima of the temperature profiles at $t \sim$ 500s are high compared with those at steady state ($t \sim$ 1300 to 2400s) and this is due to the residence time of the fluid over the plates being longer at startup than when the mean tank circulation is set up. The intrusions are at constant temperature with a strong linear gradient across the horizontal centreline, consistent with $B\_ > \kappa^3 / (A^3 l^4)$, the condition for a temperature gradient across the tank centre.

4.2 Switch to a Stabilising Forcing

In the end region the established interior flow under the unstable regime is collapsing at $t/t_f \approx 0.15$ after switching (Fig 4a). The expected decay time (t_i) of this flow is $t_i / t_f \sim N^{-1} / t_f \sim 1$. Note the start of stable counterflow on the surface of the plate. Fig 4b at $t/t_f \approx 3$ shows significant decay of the established interior flow,

with stable flow clearly exiting from the now hot plate. The thickness was measured to be 10mm compared with 12mm predicted by (5) above. Discharge velocity, measured to be 0.7mms^{-1}, compares with 0.7mms^{-1} predicted by (6) above.

The right hand end of Fig. 4b implies a four layer profile of the interior horizontal velocity - a substantially decayed remnant interior flow augmented by the intrusions derived from the stable convection.

The temperature field shown in Fig 5 spans $t/t_f \approx 0.25$ to 6 after the switch to stabilising forcing, with $t/t_f \approx 0.25$ to 4 corresponding with the stabilising condition. The residual recirculating flow responds to the lack of turbulent heat flux at $t_f/4$. From about 3700s the intrusions derived from the stable convection are present. The longer residence times over the plate imply higher temperatures at the interior provided $B_+ > Pr^{3/2}\kappa^3/\left(A^7 l^4\right)$. Notice that the temperature profiles are almost linear, by contrast with the profiles in the unstable case.

4.3 Switch Back to a Destabilising Forcing

A further switch back to unstable convection over the end plates was carried out at 4040s. The portion of Fig. 5 spanning this condition is $t/t_f \approx 0$ to $t/t_f \approx 2.5$ after the switch. By contrast with the original start, the interior is now stratified, and the history of the temperature profile evolution is different, though the final temperature profile at 4750s is close to that at 2400s in Fig 3.

5. CONCLUSIONS AND FUTURE DIRECTIONS

Destabilising buoyancy fluxes dominate the dynamics of the recirculating flow modelled here. The character of the flow is very different with unstable convection than with stable convection. In the unstable case significant mixing occurs in the end regions and recirculating flow occupies the full depth of the tank. By contrast, the unstable case does not produce mixing or recirculating flows over the full depth of the cavity and, depending upon the time chosen between switching, the decayed residual flow from the unstable configuration might still dominate over the flow induced by subsequent stabilising buoyancy fluxes. Further experiments with switching at $O(t_f)$ and $O(t_f/10)$ are being processed and the wider parameter range of which the tank is capable will be explored.

Acknowledgment: The authors thank John Devitt who constructed the experimental facility and helped with the experiments and Rob Weymouth who helped with the experiments and with the data processing. Centre for Water Research reference ED-1008-JJS.

6. REFERENCES

Linden, P.F. & Simpson, J. (1986) Gravity-driven flows in a turbulent fluid. *J. Fluid Mech.*, **172**, 481-497.

Monismith, S., Imberger J. and Morison, M. L. (1990) Convective motions in the sidearm of a small reservoir. *Limnology and Oceanography*, **35**: 1676-1702.

Noh, Y, Fernando, H. J. S. & Ching, C. Y. (1992) Flows induced by the impingement of a two-dimensional thermal on a density interface. *J. Phys. Oceanography* **22**, 1207-1219.

Phillips, O. M. (1966) On turbulent convection currents and the circulation of the Red Sea. *Deep-Sea Res.* **13**, 1149-1160.

Stevens, C. L. and Coates, M. J. (1994) A maximised cross-correlation technique for resolving velocity fields in laboratory experiments, *J. Hydr Res*, **32**, 195-212.

Sturman, J.J., Ivey, G.N. and Taylor, J.R. (1992) Convection in a long rectangular box driven by heated and cooled segments of the horizontal boundaries, *Proc. 11th Australasian Fluid Mechanics Conference*, **II**:1005-1008.

Sturman, J.J., Ivey, G.N. and Taylor, J.R. (1995) Convection in a long boxes driven by heating and cooling along the horizontal boundaries, *J. Fluid Mech.*, accepted for publication.

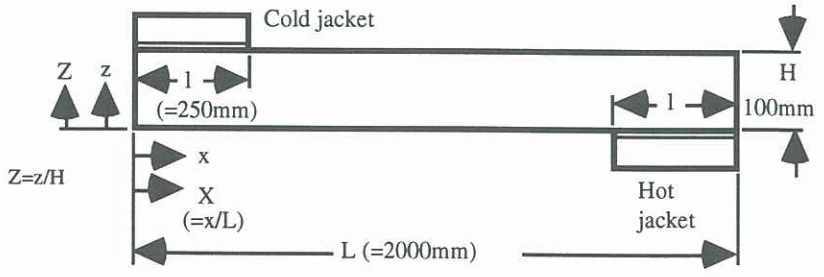

Fig. 1. Schematic diagram of tank with definition of axes. Tank dimension into page: 500mm.

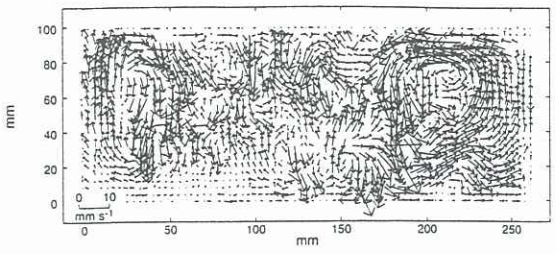

Fig. 2a $t/t_f \approx 0.13$ after start, clock time 141300

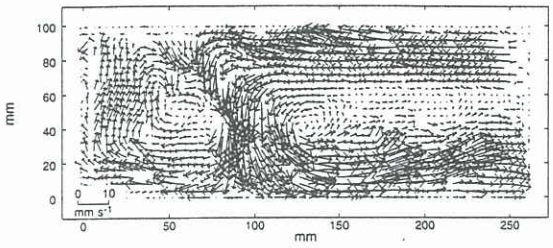

Fig. 2b $t/t_f \approx 0.3$ after start, clock time 141400

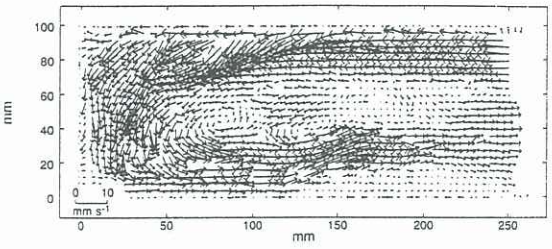

Fig. 2c $t/t_f \approx 6$ after start, clock time 145202

Fig. 2 Development of velocity field under the cold plate shortly after startup with the negative buoyancy flux giving rise to unstable convection.

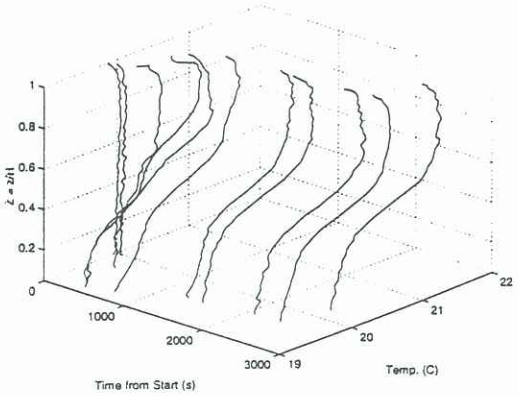

Fig. 3 The development in time of the temperature profiles at $x/L = 0.5$. At 2400s the buoyancy flux is switched at the ends to give rise to stable convection following the initially unstable convection.

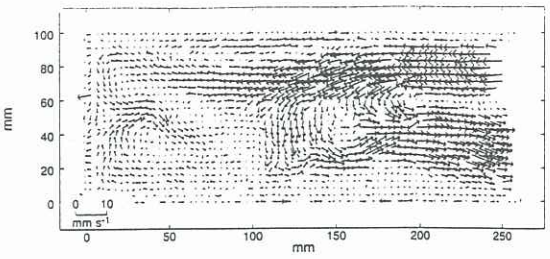

Fig. 4a $t/t_f \approx 0.15$ after switch, clock time 145300

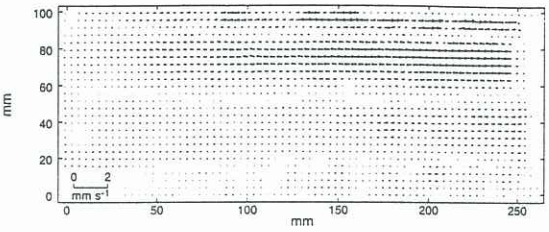

Fig. 4b $t/t_f \approx 3$ after switch, clock time 151510

Fig. 4 Development of velocity field under the cold plate following a switch from negative to positive buoyancy flux giving rise to stable convection.

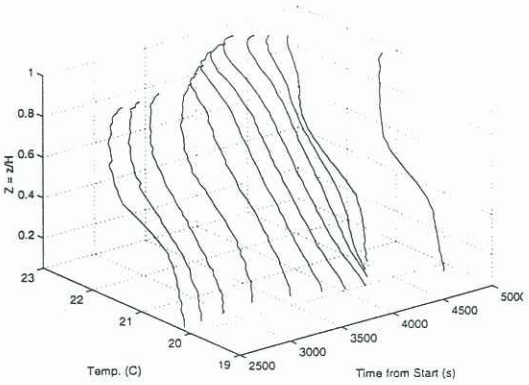

Fig. 5 The further development in time of the temperature profiles at $x/L = 0.5$. At 4040s the buoyancy flux is switched at the ends to give rise to unstable convection following the previously stable convection.